Electronic Research Archive

ERA, 31(7): 4248–4265.
DOI: 10.3934/era.2023216
Received: 23 March 2023
Revised: 02 May 2023
Accepted: 06 May 2023
Published: 01 June 2023

http://www.aimspress.com/journal/era

Research article

Application of the B-spline Galerkin approach for approximating the time-fractional Burger's equation

Akeel A. AL-saedi and Jalil Rashidinia*

School of Mathematics and Computer Science, Iran University of Science & Technology, Tehran 16846-13114, Iran

* **Correspondence:** Email: rashidinia@iust.ac.ir.

Abstract: This paper presents a numerical scheme based on the Galerkin finite element method and cubic B-spline base function with quadratic weight function to approximate the numerical solution of the time-fractional Burger's equation, where the fractional derivative is considered in the Caputo sense. The proposed method is applied to two examples by using the L_2 and L_∞ error norms. The obtained results are compared with a previous existing method to test the accuracy of the proposed method.

Keywords: time-fractional Burger's equation; Caputo derivative; B-spline Galerkin method; different weight function

1. Introduction

Fractional calculus (FC) theory was proposed by N. H. Abel and J. Liouville, and a description of their work is presented in [1]. By using FC, integer derivatives, and integrals can be generalized to real or variable derivatives and integrals. FC is studied since fractional differential equations (FDEs) are better suited to modeling natural physics processes and dynamic systems than integer differential equations. Furthermore, FDEs that incorporate memory effects are better suited to describing natural processes that have memory and hereditary properties. In other words, because fractional derivatives have memory effects, FDEs are more accurate in describing physical phenomena with memory or hereditary characteristics. There was a trend to consider FC to be an esoteric theory with no application until the last few years. Now, more and more researchers are investigating how it can be applied to economics, control system and finance. As a result, many fractional order differential operators were

developed, such as Hadamard, Riemann-Liouville, Caputo, Riesz, Grünwald-Letnikov, and variable order differential operators. The researchers have devoted considerable effort to solving FDEs numerically so that they can be applied to a variety of problems [2–20]. Several numerical approaches have been proposed in the literature, including eigenvector expansion, the fractional differential transform technique [21], the homotopy analysis technique [22], the homotopy perturbation transform technique [23], the generalized block pulse operational matrix technique [24] and the predictor-corrector technique [25]. In addition, the use of Legendre wavelets to integrate and differentiate fractional order matrices has been suggested as a numerical method [26,27].

In this paper, we study the numerical solution of the time-fractional Burger's equation (TFBE) [28] as follows:

$$\frac{\partial^{\gamma} U(x,t)}{\partial t^{\gamma}} + U(x,t)\frac{\partial U(x,t)}{\partial x} - v\frac{\partial^2 U(x,t)}{\partial x^2} = f(x,t), \tag{1}$$

which is subject to the following boundary conditions (BCs):

$$U(a,t) = l_1(t), U(b,t) = l_2(t), \quad a \le x \le b, \ \ t \in [0, t_f], \tag{2}$$

and the following initial condition (IC):

$$U(x,0) = g(x) \text{ and } a \le x \le \text{b}, \tag{3}$$

in which $0 < \gamma \le 1$ is a parameter representing the order of the fractional time, v denotes a viscosity parameter and $g(x), l_1(t)$ and $l_2(t)$ are given functions of their argument. The TFBE is a kind of sub-diffusion convection, which is widely adopted to describe many physical problems such as unidirectional propagation of weakly nonlinear acoustic waves, shock waves in flow systems, viscous media, compressible turbulence, electromagnetic waves and weak shock propagation [29–31]. In recent years, there has been some technique development in the study of Burger's equation: an implicit difference scheme and algorithm implementation [32], pointwise error analysis of the third-order backward differentiation formula (BDF3) [33], pointwise error estimates of a compact difference scheme [34], efficient (BDF3) finite-difference scheme [35], semi-analytical methods [36], composite spectral methods [37], least-squares methods [38], geometric analysis methods [39], error and stability estimate techniques [40].

Definition 1. Suppose that m is the smallest integer exceeding γ; the Caputo time fractional derivative operator of order $\gamma > 0$ can be defined as follows [41]:

$$CD_{0,t}^{\gamma} u(x,t) = \begin{cases} \dfrac{\partial^m u(x,t)}{\partial t^m} & \gamma = m \in N \\ \dfrac{1}{\Gamma(m-\gamma)} \displaystyle\int_0^t (t-\omega)^{m-\gamma-1} \frac{\partial^m u(x,\omega)}{\partial \omega^m} d\omega, & m-1 < \gamma < m, m \in N, \end{cases} \tag{4}$$

where $u(x,t)$ is the unknown function that is $(m-1)$ times continuously differentiable and $\Gamma(.)$ denotes the usual gamma function. The finite-element method has been an important method for solving both ordinary and partial differential equation, therefore, in recent research, it has been applied to solve the TFBE. In what follows, we describe the solution process by using the finite-element scheme for solving the TFBE.

2. Cubic B-Spline Galerkin method (CBSGM) with a quadratic weight function:

To discretize the TFBE (1), first let us define the cubic B-spline base function. We partition the interval $[a, b]$, which represents the solution domain of (1) into M uniformly spaced points x_m such that $a = x_0 < x_1 < \cdots < x_{M-1} < x_M = b$ and $h = (x_{m+1} - x_m)$. Then, the cubic B-spline $C_m(x), (m = -1(1)(M+1)$, at the knots x_m which form basis on the solution interval $[a, b]$, is defined as follows [42]:

$$C_m(x) = \frac{1}{h^3}\begin{cases} (x - x_{m-2})^3, & \text{if } x \in [x_{m-2}, x_{m-1}], \\ h^3 + 3h^2(x - x_{m-1}) + 3h(x - x_{m-1})^2 - 3(x_{m+1} - x)^3, & \text{if } x \in [x_{m-1}, x_m], \\ h^3 + 3h^2(x_{m+1} - x) + 3h(x_{m+1} - x)^2 - 3(x_{m+1} - x)^3, & \text{if } x \in [x_m, x_{m+1}], \\ (x_{m+2} - x)^3, & \text{if } x \in [x_{m+1}, x_{m+2}], \\ o, & \text{otherwise.} \end{cases} \tag{5}$$

where the set of cubic B-splines $(C_{-1}(x), C_0(x), \ldots, C_M(x), C_{M+1}(x))$ is a basis for the functions defined over interval $[a, b]$. Thus, the numerical solution $U_M(x, t)$ to the analytic solution $U(x, t)$ can be illustrated as

$$U_M(x, t) = \sum_{m=-1}^{M+1} \sigma_m(t) C_m(x), \tag{6}$$

where $\sigma_m(t)$ are unknown time-dependent parameters to be determined from the initial, boundary and weighted residual conditions. Since each cubic B-spline covers four consecutive elements, each element $[x_m, x_{m+1}]$ is also covered by four cubic B-splines. So, the nodal values U_m and its first and second derivatives U'_m, U''_m can be respectively computed in terms of the element parameter $\sigma_m(t)$,at the knot x_m as follows:

$$\begin{aligned} U_m &= \sigma_{m-1} + 4\sigma_m + \sigma_{m+1}, \\ U'_m &= \frac{3}{h}(\sigma_{m-1} - \sigma_{m+1}), \\ U''_m &= \frac{6}{h^2}(\sigma_{m-1} - 2\sigma_m + \sigma_{m+1}), \end{aligned} \tag{7}$$

and by means of the local coordinate transformation [43] as follows:

$$h\eta = x - x_m, \quad 0 \le \eta \le 1. \tag{8}$$

A cubic B-spline shape function in terms of η over the element $[x_m, x_{m+1}]$ is formulated as:

$$\begin{aligned} C_{m-1} &= (1 - \eta)^3, \\ C_{m-1} &= 1 + 3(1 - \eta) + 3(1 - \eta)^2 - 3(1 - \eta)^3, \\ C_{m+1} &= 1 + 3\eta + 3\eta^2 - 3\eta^3, \\ C_{m+2} &= \eta^3 \end{aligned} \tag{9}$$

and the variation of $U_M(\eta,t)$ over the typical element $[x_m, x_{m+1}]$ is represented as

$$U_M(x,t) = \sum_{j=m-1}^{m+2} \sigma_j(t) C_j(\eta), \tag{10}$$

in which B-splines $C_{m-1}(\eta), C_m(\eta), C_{m+1}(\eta)$, $C_{m+2}(\eta)$ and $\sigma_{m-1}(t)$, $\sigma_m(t), \sigma_{m+1}$ and $\sigma_{m+2}(t)$ are element shape functions and element parameters, respectively.

Based on the Galerkin's method with weight function $W(x) > 0$, we get the following weak formula of (1):

$$\int_a^b W\left(\frac{\partial^\gamma U}{\partial t^\gamma} + U\frac{\partial U}{\partial x} - v\frac{\partial^2 U}{\partial x^2}\right)dx = \int_a^b W f(x,t); \tag{11}$$

using transformation (8) and by apply partial integration we obtain:

$$\int_0^1 \left(W\frac{\partial^\gamma U}{\partial t^\gamma} + \lambda W\frac{\partial U}{\partial \eta} + \Phi\frac{\partial W}{\partial \eta}\frac{\partial U}{\partial \eta}\right)d\eta = \Phi W\frac{\partial U}{\partial \eta}\Big|_0^1 + \int_a^b W \mathbb{F}(\eta,t)d\eta, \tag{12}$$

where $\lambda = \frac{1}{h}\hat{U}$, $\Phi = \frac{v}{h^2}$ and $\hat{U} = U(\eta,t)$ which is considered to be a constant on an element to simplify the integral [43]; replace the weight function W by quadratic B-spline $B_{\boldsymbol{m}}(\boldsymbol{x})$, m $= -1(1)M$, at the knots x_m, which forms a basis on the solution interval $[a,b]$, introduced as follows [44]:

$$B_m(x) = \frac{1}{h^2}\begin{cases} (x_{m+2}-x)^2 - 3(x_{m+1}-x)^2 + 3(x_m-x)^2, & \text{if } x \in [x_{m-1}, x_m], \\ (x_{m+2}-x)^2 - 3(x_{m+1}-x)^2, & \text{if } x \in [x_m, x_{m+1}], \\ (x_{m+2}-x)^2, & \text{if } x \in [x_{m+1}, x_{m+2}], \\ 0, & \text{otherwise.} \end{cases} \tag{13}$$

where $(B_{-1}(x), B_0(x), \ldots, B_M(x))$ is the set of splines for the basis of functions introduced on $[a,b]$. The numerical solution $U_M(x,t)$ to the analytic solution $U(x,t)$ is expanded by

$$U_M(x,t) = \sum_{m=-1}^{M} \vartheta_m(t) B_m(x), \tag{14}$$

where ϑ_m are unknown time-dependent parameters, and by using local coordinate transformation (8), the quadratic B-spline shape functions for the typical element $[x_m, x_{m+1}]$ are given as

$$\begin{aligned} B_{m-1} &= (1-\eta)^2 \\ B_m &= 1 + 2\eta - 2\eta^2 \\ B_{m+1} &= \eta^2 \end{aligned} \tag{15}$$

The variation of the function $U(\eta,t)$ is approximated by

$$U_M(\eta,t) = \sum_{i=m-1}^{m+1} \vartheta_i(t) B_i(\eta), \tag{16}$$

where $\vartheta_{m-1}(t)$, $\vartheta_m(t)$ and $\vartheta_{m+1}(t)$ act as element parameters and B-splines $B_{m-1}(\eta), B_m(\eta)$ and $B_{m+1}(\eta)$ as element shape functions based on the above; (12) will be in the following form:

$$\sum_{j=m-1}^{m+2}[\int_0^1 B_i C_j d\eta]\dot{\sigma} + \sum_{j=m-1}^{m+2}[\int_0^1 (\lambda B_i C_j' + \Phi B_i' C_j')d\eta - \Phi B_i C_j'|_0^1]\sigma$$

$$= \int_0^1 B_i \, \mathbb{F}(\eta, t)d\eta, \qquad i = m-1, m, m+1, \tag{17}$$

in which "Dot" represents the σth fractional derivative with respect to time. We can write (17) in matrix notation as follows:

$$X_{ij}^e \dot{\sigma}^e + (\lambda Y_{ij}^e + \Phi(Z_{ij}^e - Q_{ij}^e))\sigma^e = E_i^e, \tag{18}$$

in which $\sigma^e = (\sigma_{m-1}, \sigma_m, \sigma_{m+1}, \sigma_{m+2})^T$ are the element parameters. The element matrices $X_{ij}^e, Y_{ij}^e, Z_{ij}^e, Q_{ij}^e$ and E_i^e are rectangular 3×4 matrices introduced through the following integrals:

$$X_{ij}^e = \int_0^1 B_i C_j \, d\eta = \frac{1}{60}\begin{bmatrix} 10 & 71 & 38 & 1 \\ 19 & 221 & 221 & 19 \\ 1 & 38 & 71 & 10 \end{bmatrix},$$

$$Y_{ij}^e = \int_0^1 B_i C_j' \, d\eta = \frac{1}{10}\begin{bmatrix} -6 & -7 & 12 & 1 \\ -13 & -41 & 41 & 13 \\ -1 & -12 & 7 & 6 \end{bmatrix},$$

$$Z_{ij}^e = \int_0^1 B_i' C_j' \, d\eta = \frac{1}{2}\begin{bmatrix} 3 & 5 & -7 & -1 \\ -2 & 2 & 2 & -2 \\ -1 & -7 & 5 & 3 \end{bmatrix},$$

$$Q_{ij}^e = B_i C_j' \, |_0^1 \; = 3\begin{bmatrix} 1 & 0 & -1 & 0 \\ 1 & -1 & -1 & 1 \\ 0 & -1 & 0 & 1 \end{bmatrix} \text{ and}$$

$$E_i^e = \int_0^1 B_i \, \mathbb{F}(\eta, t)d\eta,$$

where i and j take only the values $(m-1, m, m+1)$ and $(m-1, m, m+1, m+2)$ respectively, and a lumped value for λ is defined by $\lambda = \frac{1}{2h}(\sigma_{m-1} + 5\sigma_m + 5\sigma_{m+1} + \sigma_{m+2})$.

By assembling all contributions from all elements, we get the following matrix equation:

$$X\dot{\sigma} + \big(\lambda Y + \Phi(Z - Q)\big)\sigma = E, \tag{19}$$

where $\sigma = (\sigma_{-1}, \sigma_0, \sigma_1, \dots, \sigma_M, \sigma_{M+1})^T$ denotes a global element parameter. The matrices X, Z and Y represent rectangular, septa-diagonal and every sub-diagonal matrices, which include the following forms:

$$X = \frac{1}{60}(1, 57, 302, 302, 57, 1, 0),$$

$$Z = \frac{1}{2}(-1, -9, 10, 10, -9, \ -1, 0),$$

$$\lambda Y = \frac{1}{10}(-\lambda_1, -12\lambda_1 - 13\lambda_2, 7\lambda_1 - 41\lambda_2 - 6\lambda_3, 6\lambda_1 + 41\lambda_2 - 7\lambda_3, 13\lambda_2 + 12\lambda_3, \lambda_3, 0),$$

in which,

$$\lambda_1 = \frac{1}{2h}(\sigma_{m-2} + 5\sigma_{m-1} + 5\sigma_m + \sigma_{m+1}),$$

$$\lambda_2 = \frac{1}{2h}(\sigma_{m-1} + 5\sigma_m + 5\sigma_{m+1} + \sigma_{m+2}),$$

$$\lambda_3 = \frac{1}{2h}(\sigma_m + 5\sigma_{m+1} + 5\sigma_{m+2} + \sigma_{m+3}).$$

Following [45], we can approximate the temporal Caputo derivative with the help of the $L1$ formula:

$$\frac{d^\gamma f(t)}{dt^\gamma}\Big|_{t_f} = \frac{(\Delta t)^{-\gamma}}{\Gamma(2-\gamma)} \sum_{k=0}^{m-1} b_k^\gamma [f(t_{m-k} - f(t_{m-1k})] + O(\Delta t)^{2-\gamma},$$

where $b_k^\gamma = (k+1)^{1-\gamma} - k^{1-\gamma}$ and $\Delta t = \frac{t_f - 0}{N}$, and $t_f = n(\Delta t), n = 0,1, \dots N,$ where N represents a positive integer. Now, we recall the following lemma.

Lemma 1: Suppose that $0 < \gamma < 1 \; and \; b_k^\gamma = (k+1)^{1-\gamma} - k^{1-\gamma}, k = 0,1, \dots; then, 1 = b_0^\gamma > b_1^\gamma > \cdots > b_k^\gamma \to 0, as \; k \to \infty$ [46].

Then, we can we write the parameter $\dot{\sigma_m}$ as follows:

$$\dot{\sigma_m} = \frac{d^\gamma \sigma}{dt^\gamma} = \frac{(\Delta t)^{-\gamma}}{\Gamma(2-\gamma)} \sum_{k=0}^{m-1} b_k^\gamma [(\sigma_{m-1}^{n-k+1} - \sigma_{m-1}^{n-k}) + 4(\sigma_m^{n-k+1} - \sigma_m^{n-k}) + (\sigma_{m+1}^{n-k+1} - \sigma_{m+1}^{n-k})] + O(\Delta t)^{2-\gamma}, \qquad b_k^\gamma = (k+1)^{1-\gamma} - k^{1-\gamma},$$

while the parameter σ by the Crank-Nicolson scheme, is as follows:

$$\sigma_m = \frac{1}{2}(\sigma_m^n + \sigma_m^{n+1}).$$

Substitution both parameters above into (18), we obtain the $(M+2) \times (M+3)$ matrix system:

$$\left[X+\frac{[(\Delta t)^{-\gamma}\Gamma(2-\gamma)(\lambda Y+\Phi(Z-Q)]}{2}\right]\sigma^{n+1}$$

$$=\left[X-\frac{[(\Delta t)^{-\gamma}\Gamma(2-\gamma)(\lambda Y+\Phi(Z-Q)]}{2}\right]\sigma^{n}$$

$$-X\sum_{k=1}^{n}b_k^{\gamma}\left[\left(\sigma_{m-1}^{n-k+1}-\sigma_{m-1}^{n-k}\right)+4\left(\sigma_{m}^{n-k+1}-\sigma_{m}^{n-k}\right)+\left(\sigma_{m+1}^{n-k+1}-\sigma_{m+1}^{n-k}\right)\right]$$
$$+(\Delta t)^{-\gamma}\Gamma(2-\gamma)E\,, \tag{20}$$

where $\sigma=(\sigma_{m-2}+\sigma_{m-1}+\sigma_m+\sigma_{m+1}+\sigma_{m+1}+\sigma_{m+2}+\sigma_{m+3})^T$; to make the matrix equation be square, we need to find an additional constraint of BC (2) and their second derivatives and we obtain discard σ_{-1} from system (20) as follows:

$$\sigma_{-1}(t)=-4\sigma_0(t)-\sigma_1(t)+U(x_0,t);$$

the variables σ_{-1}^n and σ_{M+1}^n can be ignored from system (20) and then the system can be converted to an $(M+1)\times(M+1)$ matrix system. The initial vector of parameter $\sigma^0=(\sigma_0^0,\sigma_1^0,\dots,\sigma_M^0)$ should be obtained to iterate system (20); the approximation of (6) has been reformulated on the interval $[a,b]$ when time $t=0$ as follows:

$$U_N(x,0)=\sum_{m=0}^{M}C_m\sigma_m^0,$$

where $U(x,0)$ fulfills the following equation at node x_m:

$$U_M(x_m,0)=U(x_m,0),\qquad m=0,1,\dots,M+1$$
$$U_M'(x_0,0)=U'(x_M,0)=0,$$
$$U_M''(x_0,0)=U''(x_M,0)=0.$$

Therefore, we can obtain the following system:

$$\begin{bmatrix}\sigma_0^0 & 6 & 0 & 0 & & & & & 0\\ \sigma_1^0 & 1 & 4 & 1 & & & & & 0\\ \vdots & & 1 & 4 & 4 & & & & \\ & & & & \ddots & \ddots & & & \\ \sigma_{M-1}^0 & & & & & \ddots & 1 & 4 & 1\\ \sigma_M^0 & 0 & & & & & & 0 & 6\end{bmatrix}\begin{bmatrix}\sigma_0^0\\ \sigma_1^0\\ \vdots\\ \sigma_{M-1}^0\\ \sigma_M^0\end{bmatrix}=\begin{bmatrix}U(x_0,0)-\frac{h^2}{6}g^{"}(a)\\ U(x_1,0)\\ \vdots\\ U(x_{M-1},0)\\ U(x_M,0)-\frac{h^2}{6}g^{"}(b)\end{bmatrix}$$

and we solve this identity matrix by applying the Jain algorithm [47].

3. Stability analysis

This section adopts the von Neumann stability analysis to investigate the stability of approximation obtained by scheme (20). First, we introduce the recurrence relationship between successive time levels relating unknown element parameters $\sigma_m^{n+1}(t)$, as follows:

$$\begin{aligned}
&q_1\sigma_{m-2}^{n+1} + q_2\sigma_{m-1}^{n+1} + q_3\sigma_m^{n+1} + q_4\sigma_{m+1}^{n+1} + q_5\sigma_{m+2}^{n+1} + q_6\sigma_{m+3}^{n+1} \\
&= q_6\sigma_{m-2}^{n} + q_5\sigma_{m-1}^{n} + q_4\sigma_m^{n} + q_3\sigma_{m+1}^{n} + q_2\sigma_{m+2}^{n} + q_1\sigma_{m+3}^{n} \\
&- 20\sum_{k=1}^{n} b_k^{\gamma}\Big[\big(\big(\sigma_{m-2}^{n-k+1} - \sigma_{m-2}^{n-k}\big) + 4\big(\sigma_{m-2}^{n-k+1} - \sigma_{m-2}^{n-k}\big) + \big(\sigma_{m-2}^{n-k+1} - \sigma_{m-2}^{n-k}\big)\big) \\
&+ 57\big(\big(\sigma_{m-1}^{n-k+1} - \sigma_{m-1}^{n-k}\big) + 4\big(\sigma_{m-1}^{n-k+1} - \sigma_{m-1}^{n-k}\big) + +\big(\sigma_{m-1}^{n-k+1} - \sigma_{m-1}^{n-k}\big)\big) \\
&+ 302\big(\big(\sigma_m^{n-k+1} - \sigma_m^{n-k}\big) + 4\big(\sigma_m^{n-k+1} - \sigma_m^{n-k}\big) + \big(\sigma_m^{n-k+1} - \sigma_m^{n-k}\big)\big) \\
&+ 302\Big(\big(\sigma_{m+1}^{n-k+1} - \sigma_{m+1}^{n-k}\big) + 4\big(\sigma_{m+1}^{n-k+1} - \sigma_{m+1}^{n-k}\big) + \big(\sigma_{m+1}^{n-k+1} - \sigma_{m+1}^{n-k}\big)\Big) \\
&+ 57\Big(\big(\sigma_{m+2}^{n-k+1} - \sigma_{m+2}^{n-k}\big) + 4\big(\sigma_{m+2}^{n-k+1} - \sigma_{m+2}^{n-k}\big) + \big(\sigma_{m+2}^{n-k+1} - \sigma_{m+2}^{n-k}\big)\Big) \\
&+ \big(\big(\sigma_{m+3}^{n-k+1} - \sigma_{m+3}^{n-k}\big) + 4\big(\sigma_{m+3}^{n-k+1} - \sigma_{m+3}^{n-k}\big) \\
&+ \big(\sigma_{m+3}^{n-k+1} - \sigma_{m+3}^{n-k}\big)\big)\Big]
\end{aligned} \tag{21}$$

where

$$q_1 = 20 - 300\Phi\alpha - 60\lambda\alpha,\ \ q_2 = 1140 - 2700\Phi\alpha - 1500\lambda\alpha,\ \ q_3 = 6040 + 3000\Phi\alpha - 2400\lambda\alpha$$

$$q_4 = 6040 + 3000\Phi\alpha + 2400\lambda\alpha,\ \ q_5 = 1140 - 2700\Phi\alpha + 1500\lambda\alpha,\ \ q_6 = 20 - 300\Phi\alpha + 60\lambda\alpha$$

and $\alpha = (\Delta t)^{-\gamma}\Gamma(2-\gamma)$.

The growth factor of the typical Fourier mode is defined as

$$\sigma_m^n = \xi^n e^{i\beta mh} \tag{22}$$

where, $i = \sqrt{-1},\ \ \beta$ is a mode number and h is the element size. Substitution of (22) into (21) yields

$$\begin{aligned}
&\xi^{n+1}\big(q_1e^{-2i\beta h} + q_2e^{-i\beta h} + q_3 + q_4e^{i\beta h} + q_5e^{2i\beta h} + q_6e^{3i\beta h}\big) = \\
&\xi^{n}\big(q_6e^{-2i\beta h} + q_5e^{-i\beta h} + q_4 + q_3e^{i\beta h} + q_2e^{2i\beta h} + q_1e^{3i\beta h}\big) \\
&-20\sum_{k=1}^{n} b_k^{\gamma}\Big[\Big(\big(\sigma_{m-2}^{n-k+1} - \sigma_{m-2}^{n-k}\big) + 4\big(\sigma_{m-2}^{n-k+1} - \sigma_{m-2}^{n-k}\big) + \big(\sigma_{m-2}^{n-k+1} - \sigma_{m-2}^{n-k}\big)\Big)\big(e^{-2i\beta h}302 \\
&+ 302e^{i\beta h} + 57e^{2i\beta h} + e^{2i\beta h}\big)\Big];
\end{aligned} \tag{23}$$

let $\xi^{n+1} = \ddot{\Upsilon}\xi^n$ and assume that $\ddot{\Upsilon} \equiv \ddot{\Upsilon}(\theta)$ is independent of time, therefore, we can write $\ddot{\Upsilon}$ as follows:

$$\ddot{\Upsilon} = \frac{A - iB}{A + iB},$$

where

$$A = (6040 + 3000\Phi\alpha)\cos\left(\frac{\theta}{2}\right)h + (1140 - 2700\Phi\alpha)\cos\left(\frac{3\theta}{2}\right)h + (20 - 300\Phi\alpha)\cos\left(\frac{5\theta}{2}\right)h,$$

$$B = (2400\lambda\alpha)\sin\left(\frac{\theta}{2}\right)h + +(1500\lambda\alpha)\sin\left(\frac{3\theta}{2}\right)h + (60\lambda\alpha)\sin\left(\frac{\theta}{2}\right)h,$$

Obviously note that $|\ddot{\Upsilon}| \leq 1$. Therefore, according to the Fourier condition, the scheme (20) is unconditionally stable.

4. Numerical results

This section introduces two numerical examples, which highlight numerical results for the TFBE with different IC and BCs given by the CBSGM with quadratic weight function. In this section, we use the L_2 and L_∞ to calculate the accuracy of the CBSGM with a quadratic weight function, which has been employed in this study; we will also show how the analytical results and the numerical results are close to each other. To do this, first we will find the exact solutions to the problem (1) by applying the following problems; then, we compare the results with the numerical solution obtained from the given method. To this aim, the $\boldsymbol{L}_\infty$ and $\boldsymbol{L_2}$ error norms are respectively defined as [48]

$$L_\infty = \left\| U - U_M \right\|_\infty \cong \max_j \left| U_j - (U_M)_j \right|,$$

$$L_2 = \left\| U - U_M \right\|_2 \cong \sqrt{h \sum_{j=0}^{M} \left| U_j - (U_M)_j \right|^2}$$

where U and U_M represent the exact solution and numerical solution, respectively.

Example 1: Let us consider the TFBE (1) with the BCs

$$U(O,t) = l_1(t) = t^2, \qquad U(1,t) = l_2(t) = -t^2, \qquad t \geq 0,$$

and IC

$$U(x,0) = g(x) = 0, \qquad 0 \leq x \leq 1,$$

such that the forcing term $f(x,t)$ is achieved as [45]

$$f(x,t) = \frac{2t^{2-\gamma}e^x}{\Gamma(3-\gamma)} + t^4 e^{2x} - vt^2 e^x,$$

where the analytic solution is obtained as

$$U(x,t) = t^2 e^x.$$

Numerical results are reported in Tables 1–3 and Figure 1. Table 1 lists the numerical solutions and the L_2 and L_∞ error norms with $\gamma = 0.5,\ \Delta t = 0.0025,\ t_f = 0.05$ and $v = 1$ for various numbers of partitions M. As seen in Table 1, we notice that when the number of partitions M are increased, the L_∞ and L_2 error norms will decrease considerably. Table 2 displays the numerical solutions with $\gamma = 0.5,\ M = 40,\ t = 1,\ t_f = 0.05$ and $v = 1$ for various values of Δt. In view of Table 2, we can see that when Δt decreases, the L_∞ and L_2 error norms decrease, as was expected. Table 3 shows the numerical solutions with $\Delta t = 0.00025,\ M = 40,\ t = 1,\ t_f = 0.05,\ v = 1$ for various values of γ. As observed in Table 3, the L_∞ and L_2 error norms decrease when γ increases. A comparison between the results of our proposed strategy and two other methods is demonstrated in detail, the researchers of which relied on their work on a weight function corresponding to the spline function in terms of degree; see [44,45]. Figure 1 represents the surfaces of the exact and numerical solutions of the TFBE in Example (1).

Table 1. Numerical solutions with $\gamma = 0.5,\ \Delta t = 0.0025,\ t_f = 0.05,\ v = 1$ for various numbers of partitions M.

x	M = 10	M = 20	M = 40	M = 80	Exact
0.0	0.000000	0.000000	0.000000	0.000000	0.000000
0.1	1.104360	1.105211	1.105166	1.105122	1.105101
0.2	1.222151	1.222040	1.221593	1.221555	1.221511
0.3	1.351010	1.350426	1.350012	1.349831	1.349789
0.4	1.493377	1.492288	1.491990	1.491910	1.491844
0.5	1.650589	1.650001	1.649822	1.648889	1.648731
0.6	1.824211	1.823336	1.822449	1.822214	1.822110
0.7	2.015587	2.014111	2.013822	2.013776	2.013692
0.8	2.227577	2.226110	2.225699	2.225611	2.225562
0.9	2.461410	2.461101	2.460893	2.459550	2.459491
1.0	2.718202	2.718202	2.718202	2.718202	2.718202
$\boldsymbol{L_2 \times 10^3}$	1.631895	0.440555	0.160761	0.062504	
$\boldsymbol{L_2 \times 10^3}$ **[44]**	1.764966	0.465690	0.167743	0.095754	
$\boldsymbol{L_2 \times 10^3}$ **[45]**	1.632995	0.447720	0.161833	0.082624	
$\boldsymbol{L_\infty \times 10^3}$	2.291578	0.64933	0.206677	0.032882	
$\boldsymbol{L_\infty \times 10^3}$ **[49]**	3.101238	0.812842	0.209495	0.069208	
$\boldsymbol{L_\infty \times 10^3}$ **[50]**	2.296683	0.625018	0.207352	0.033125	

Table 2. Numerical solutions with $\gamma = 0.5,\ M = 40,\ t = 1,\ t_f = 0.05,\ v = 1$ for various values of Δt.

x	Δt = 0.005	Δt = 0.001	Δt = 0.0005	Δt = 0.00025	Exact
0.0	0.000000	0.000000	0.000000	0.000000	0.000000
0.1	1.105216	1.105211	1.105199	1.105186	1.105150
0.2	1.221701	1.221601	1.221511	1.221445	1.221389
0.3	1.350321	1.350188	1.350141	1.350110	1.349998
0.4	1.492461	1.492211	1.492101	1.491879	1.491804
0.5	1.649485	1.649112	1.648961	1.648822	1.648690
0.6	1.822941	1.822675	1.822431	1.822310	1.822144
0.7	2.014601	2.014201	2.014055	2.013979	2.013788
0.8	2.226288	2.226001	2.225812	2.225699	2.225528
0.9	2.260100	2.459980	2.459862	2.459785	2.459655
1.0	2.718202	2.718202	2.718202	2.718202	2.718202
$\boldsymbol{L_2 \times 10^3}$	0.659999	0.374901	0.232591	0.092489	
$\boldsymbol{L_2 \times 10^3}$ [44]		0.176195	0.068869		
$\boldsymbol{L_2 \times 10^3}$ [45]		0.375012	0.232768	0.092624	
$\boldsymbol{L_\infty \times 10^3}$	0.936512	0.529997	0.326112	0.132945	
$\boldsymbol{L_\infty \times 10^3}$ [44]		0.665419	0.411883		
$\boldsymbol{L_\infty \times 10^3}$ [45]		0.530231	0.328303	0.133125	

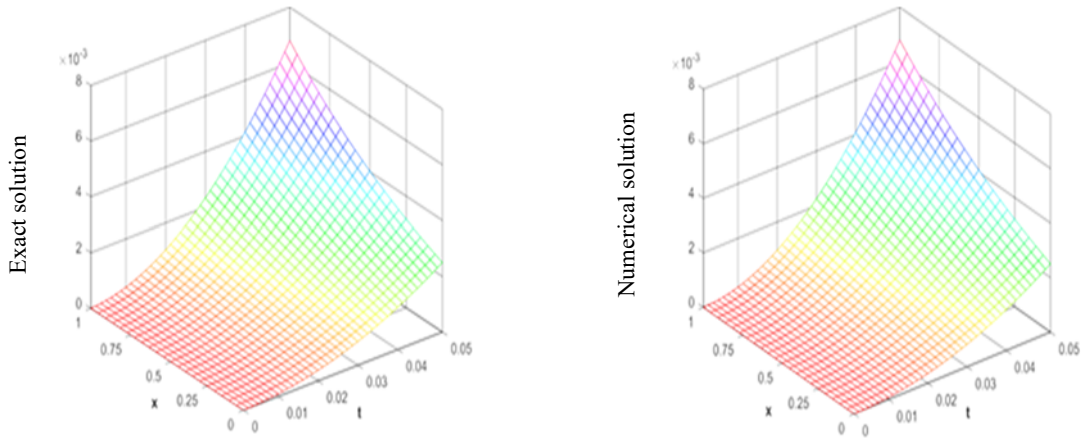

Figure 1. The surfaces of the exact and numerical solutions of the TFBE in Example (1).

Table 3. Numerical solutions with $\Delta t = 0.00025,\ M = 40,\ t = 1,\ t_f = 0.05,\ v = 1$ for various values of γ.

x	$\gamma = 0.10$	$\gamma = 0.25$	$\gamma = 0.75$	$\gamma = 0.90$	Exact
0.0	0.000000	0.000000	0.000000	0.000000	0.000000
0.1	1.105068	1.104981	1.104890	1.104899	1.104882
0.2	1.221701	1.221601	1.221511	1.221445	1.221389
0.3	1.350321	1.350188	1.350141	1.350110	1.349998
0.4	1.492461	1.492211	1.492101	1.491879	1.491804
0.5	1.649485	1.649112	1.648961	1.648822	1.648690
0.6	1.822941	1.822675	1.822431	1.822310	1.822144
0.7	2.014601	2.014201	2.014055	2.013979	2.013788
0.8	2.226288	2.226001	2.225812	2.225699	2.225528
0.9	2.260100	2.459980	2.459862	2.459785	2.459655
1.0	2.718202	2.718202	2.718202	2.718202	2.718202
$\boldsymbol{L_2 \times 10^3}$	0.659999	0.374901	0.232591	0.092489	
$\boldsymbol{L_2 \times 10^3}$ **[44]**	0.096733	0.090053	0.035448	0.044398	
$\boldsymbol{L_2 \times 10^3}$ **[45]**	0.167077	0.165443	0.159924	0.166085	
$\boldsymbol{L_\infty \times 10^3}$	0.936512	0.529997	0.328112	0.132945	
$\boldsymbol{L_\infty \times 10^3}$ **[44]**	0.272943	0.258623	0.124569	0.066682	
$\boldsymbol{L_\infty \times 10^3}$ **[45]**	0.235837	0.232645	0.224532	0.232565	

Example 2: Finally, we consider the TFBE (1) with the BCs

$$U(0,t) = 0, \qquad U(1,t) = 0, \qquad t \geq 0,$$

and IC

$$U(x,0) = 0, \qquad 0 \leq x \leq 1,$$

where the source term $f(x,t)$ can be obtained as [44]

$$f(x,t) = \frac{2t^{2-\gamma}\sin(2\pi x)}{\Gamma(3-\gamma)} + 2\pi t^4 \sin(2\pi x)\cos(2\pi x) + 4vt^2\pi^2 \sin(2\pi x).$$

The exact solution is

$$U(x,t) = t^2 \sin(2\pi x).$$

Table 4. Numerical solutions with $\gamma = 0.5,\ \Delta t = 0.0025,\ t_f = 0.05,\ v = 1$ for various numbers of partitions M.

x	M = 10	M = 20	M = 40	M = 80	Exact
0.0	1,000,000	1,000,000	1,000,000	1,000,000	1,000,000
0.1	0.951196	0.950876	0.951005	0.951077	0.951070
0.2	0.808211	0.808681	0.808911	0.808988	0.808978
0.3	0.587211	0.587513	0.587699	0.587761	0.587754
0.4	0.308662	0.308901	0.308987	0.309011	0.309006
0.5	0.000000	0.000000	0.000000	0.000000	0.000000
0.6	-0.308662	-0.308843	-.308931	-0.309011	-0.309006
0.7	-0.587194	-0.587501	-0.587694	-0.587737	-0.587732
0.8	-0.808205	-0.808644	-0.808823	-0.808972	-0.808970
0.9	-0.951211	-0.951661	-0.951811	-0.951965	-0.951960
1.0	-1.000000	-1.000000	-1.000000	-1.000000	-1.000000
$\boldsymbol{L_2 \times 10^3}$	0.435298	0.183971	0.041943	0.001960	
$\boldsymbol{L_2 \times 10^3}$ **[44]**			1.224329	0.177703	
$\boldsymbol{L_2 \times 10^3}$ **[45]**			2.899412	0.577143	
$\boldsymbol{L_\infty \times 10^3}$	0.731071	0.273289	0.063201	0.004168	
$\boldsymbol{L_\infty \times 10^3}$ **[44]**			1.730469	0.253053	
$\boldsymbol{L_\infty \times 10^3}$ **[45]**			4.063808	0.813220	

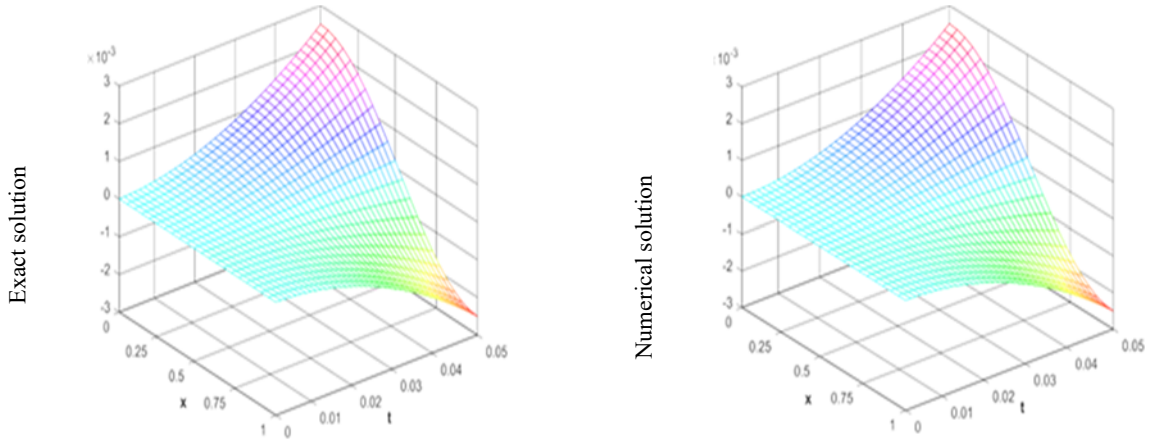

Figure 2. The surfaces of the exact and numerical solutions of the TFBE in Example (2).

Table 5: Numerical solutions with $\gamma = 0.5,\ M = 80,\ t = 1,\ t_f = 0.05,\ v = 1$ for various values of Δt.

x	$\Delta t = 0.005$	$\Delta t = 0.001$	$\Delta t = 0.0005$	$\Delta t = 0.00025$	Exact
0.0	1000000	1000000	1000000	1000000	1000000
0.1	0.951196	0.950876	0.951005	0.951077	0.951070
0.2	0.808211	0.808681	0.808911	0.808988	0.808978
0.3	0.587211	0.587513	0.587699	0.587761	0.587754
0.4	0.308662	0.308901	0.308987	0.309011	0.309006
0.5	0.000000	0.000000	0.000000	0.000000	0.000000
0.6	-0.308662	-0.308843	-.308931	-0.309011	-0.309006
0.7	-0.587194	-0.587501	-0.587694	-0.587737	-0.587732
0.8	-0.808205	-0.808644	-0.808823	-0.808972	-0.808970
0.9	-0.951211	-0.951661	-0.951811	-0.951965	-0.951960
1.0	-1.000000	-1.000000	-1.000000	-1.000000	-1.000000
$\boldsymbol{L_2 \times 10^3}$	0.124034	0.054081	0.014255	0.001960	
$\boldsymbol{L_2 \times 10^3}$ **[44]**		0.532436	0.188710		
$\boldsymbol{L_2 \times 10^3}$ **[45]**		0.359489	0.017828		
$\boldsymbol{L_\infty \times 10^3}$	0.175611	0.077465	0.028523	0.004168	
$\boldsymbol{L_\infty \times 10^3}$ **[44]**		0.753171	0.267546		
$\boldsymbol{L_\infty \times 10^3}$ **[45]**		0.512105	0.0321162		

Numerical results are represented in Tables 4 and 5 and Figure 2. Tables 4 and 5 report the numerical solutions for various numbers of partitions M and values of Δt. As seen in Tables 4 and 5, when the number of partitions M increased, the error norms L_∞ and L_2 will decrease considerably, while, in Table 5, we can see that when Δt decrease, the error norms L_∞ and L_2 decrease. Figure 2 demonstrates the surfaces of the exact and numerical solutions of the TFBE in Example (2).

5. Conclusions

This paper presented a numerical approach based on the CBSGM with a quadratic weight function for the TFBE including the time Caputo derivative. Numerical results have shown that the proposed method is an appropriate and efficient scheme for solving such problems.

Conflict of interest

The authors declare no conflict of interest.

References

1. A. Kilbas, H. M. Srivastava, J. J. Trujillo, *Theory and Applications of Fractional Differential Equations*, Elsevier, Amsterdam, 2006.
2. O. Nikan, Z. Avazzadeh, J. A. Tenreiro Machado, A local stabilized approach for approximating the modified time-fractional diffusion problem arising in heat and mass transfer, *J. Adv. Res.* **32** (2021), 45–60. https://doi.org/10.1016/j.jare.2021.03.002
3. O. Nikan, J. A. Tenreiro Machado, A. Golbabai, T. Nikazad, Numerical approach for modeling fractal mobile/immobile transport model in porous and fractured media, *Int. Commun. Heat Mass Transfer*, **111** (2020), 104443. https://doi.org/10.1016/j.icheatmasstransfer.2019.104443
4. O. Nikan, J. A. Tenreiro Machado, A. Golbabai, T. Nikazad., Numerical investigation of the nonlinear modified anomalous diffusion process, *Nonlinear Dyn.*, **97** (2019), 2757–2775. https://doi.org/10.1007/s11071-019-05160-w
5. H. Mesgarani, J. Rashidinia, Y. Esmaeelzade Aghdam, O. Nikan, Numerical treatment of the space fractional advection–dispersion model arising in groundwater hydrology, *Comput. Appl., Math.*, **40** (2021). https://doi.org/10.1007/s40314-020-01410-5
6. O. Nikan, J. A. Tenreiro Machado, A. Golbabai, Numerical solution of time-fractional fourth-order reaction-diffusion model arising in composite environments, *Appl. Math. Modell.*, **89** (2021), 819–836. https://doi.org/10.1016/j.apm.2020.07.021
7. O. Nikan, A. Golbabai, J. T. Machado, T. Nikazad, Numerical approximation of the time fractional cable model arising in neuronal dynamics, *Eng. Comput.*, **38** (2022), 155–173. https://doi.org/10.1007/s00366-020-01033-8
8. Z. Avazzadeh, O. Nikan, A. T. Nguyen, A localized hybrid kernel meshless technique for solving the fractional Rayleigh–Stokes problem for an edge in a viscoelastic fluid, *Eng. Anal. Boundary Elem.*, **146** (2023), 695–705. https://doi.org/10.1016/j.enganabound.2022.11.003
9. R. AlAhmad, Q. AlAhmad, A. Abdelhadi, Solution of fractional autonomous ordinary differential equations, *J. Math. Comput. Sci.*, **27**(2022), 59–64. http://dx.doi.org/10.22436/jmcs.027.01.05
10. O. Nikan, S. M. Molavi-Arabshai, H. Jafari, Numerical simulation of the nonlinear fractional regularized long-wave model arising in ion acoustic plasma waves, *Discrete Contin. Dyn. Syst. - S*, **14** (2021), 3685–3701. https://doi.org/10.3934/dcdss.2020466
11. Y. Cao, O. Nikan, Z. Avazzadeh, A localized meshless technique for solving 2D nonlinear integro-differential equation with multi-term kernels, *Appl. Numer. Math*., **183** (2023), 140–156. https://doi.org/10.1016/j.apnum.2022.07.018
12. A. Golbabai, O. Nikan, T. Nikazad, Numerical investigation of the time fractional mobile-immobile advection-dispersion model arising from solute transport in porous media, *Int. J. Appl. Math.*, **5** (2019), 1–22. https://doi.org/10.1007/s40819-019-0635-x
13. N. H. Can, O. Nikan, M. N. Rasoulizadeh, H. Jafari, Y. S. Gasimov, Numerical computation of the time non-linear fractional generalized equal width model arising in shallow water channel, *Therm. Sci.*, **24** (2020), 49–58.
14. T. Guo, O. Nikan, Z. Avazzadeh, W. Qiu, Efficient alternating direction implicit numerical approaches for multi-dimensional distributed-order fractional integro differential problems, *Comput. Appl. Math.*, **41** (2022), 236. https://doi.org/10.1007/s40314-022-01934-y

15. H. K. Jassim, M. A. Shareef, On approximate solutions for fractional system of differential equations with Caputo-Fabrizio fractional operator, *J. Math. Comput. Sci.*, **23** (2021), 58–66. http://dx.doi.org/10.22436/jmcs.023.01.06
16. B. Kalimbetov, E. Abylkasymova, G. Beissenova, On the asymptotic solutions of singulary perturbed differential systems of fractional order, *J. Math. Comput. Sci.*, **24**, (2022), 165–172. http://dx.doi.org/10.22436/jmcs.024.02.07
17. S. Al-Ahmad, I. M. Sulaiman, M. M. A. Nawi, M. Mamat, M. Z. Ahmad, Analytical solution of systems of Volterra integro-differential equations using modified differential transform method, *J. Math. Comput. Sci.*, **26** (2022), 1–9. http://dx.doi.org/10.22436/jmcs.026.01.01
18. A. Alia, M. Abbasb, T. Akramc, New group iterative schemes for solving the two-dimensional anomalous fractional sub-diffusion equation, *J. Math. Comput. Sci.*, **22** (2021), 119–127. http://dx.doi.org/10.22436/jmcs.022.02.03
19. T. Akram, M. Abbas, A. Ali, A numerical study on time-fractional Fisher equation using an extended cubic B-spline approximation, *J. Math. Comput. Sci*., **22** (2021), 85–96. http://dx.doi.org/10.22436/jmcs.022.01.08
20. M. Luo, W. Qiu, O. Nikan, Z. Avazzadeh, Second-order accurate, robust and efficient ADI Galerkin technique for the three-dimensional nonlocal heat model arising in viscoelasticity, *Appl. Math. Comput.*, **440** (2023), 127655. https://doi.org/10.1016/j.amc.2022.127655
21. P. Darania, A. Ebadian, A method for the numerical solution of the integro-differential equations, *Appl. Math. Comput.*, **188** (2007), 657–668. https://doi.org/10.1016/j.amc.2006.10.046
22. I. Hashim, O. Abdulaziz, S. Momani, Homotopy analysis method for fractional IVPs, *Commun. Nonlinear Sci. Numer. Simul.*, **14** (2009), 674–684. https://doi.org/10.1016/j.cnsns.2007.09.014
23. J. Gómez-Aguilar, H. Yépez-Martínez, J. Torres-Jiménez, T. Córdova-Fraga, R. Escobar-Jiménez, V. Olivares-Peregrino, Homotopy perturbation transform method for nonlinear differential equations involving to fractional operator with exponential kernel, *Adv. Differ. Equations*, **2017** (2017). https://doi.org/10.1186/s13662-017-1120-7
24. Y. Li, N. Sun, Numerical solution of fractional differential equations using the generalized block pulse operational matrix, *Comput. Math. Appl*., **62** (2011), 1046–1054, https://doi.org/10.1016/j.camwa.2011.03.032
25. K. Diethelm, N. J. Ford, A. D. Freed, A predictor-corrector approach for the numerical solution of fractional differential equations, *Nonlinear Dyn.*, **29** (2002), 3–22. https://doi.org/10.1023/A:1016592219341
26. H. Jafari, S. A. Yousefi, M. A. Firoozjaee, S. Momani, C. M. Khalique, Application of Legendre wavelets for solving fractional differential equations, *Comput. Math. Appl.*, **62** (2011), 1038–1045. https://doi.org/10.1016/j.camwa.2011.04.024
27. Z. Odibat, On Legendre polynomial approximation with the VIM or HAM for numerical treatment of nonlinear fractional differential equations, *J. Comput. Appl. Math.*, **235** (2011), 2956–2968. https://doi.org/10.1016/j.cam.2010.12.013
28. A. Yokus, D. Kaya, Numerical and exact solutions for time fractional Burgers' equation, *Nonlinear Sci. Appl.*, **10** (2017), 3419–3428. http://dx.doi.org/10.22436/jnsa.010.07.06
29. A. Esen, F. Bulut, Ö. Oruç, A unified approach for the numerical solution of time fractional Burgers' type equations, *Eur. Phys. J. Plus*, **131** (2016). https://doi.org/10.1140/epjp/i2016-16116-5

30. C. S. Liu, J. R. Chang, Recovering a source term in the time-fractional Burgers equation by an energy boundary functional equation, *Appl. Math. Lett.*, **79** (2018), 138–145. https://doi.org/10.1016/j.aml.2017.12.010
31. M. Li, O. Nikan, W. Qiu, D. Xu, An efficient localized meshless collocation method for the two-dimensional Burgers-type equation arising in fluid turbulent flows, *Eng. Anal. Boundary Elem.*, **144** (2022), 44–54. https://doi.org/10.1016/j.enganabound.2022.08.007
32. W. Qiu, H. Chen, X. Zheng, An implicit difference scheme and algorithm implementation for the one-dimensional time-fractional Burgers equations, *Math. Comput. Simul*., **166** (2019), 298–314. https://doi.org/10.1016/j.matcom.2019.05.017
33. T. Guo, M. A. Zaky, A. S. Hendy, W. Qiu, Pointwise error analysis of the BDF3 compact finite difference scheme for viscous Burgers' equations, *Appl. Numer. Math.*, **185** (2022), 260–277. https://doi.org/10.1016/j.apnum.2022.11.023
34. X. Peng, D. Xu, W. Qiu, Pointwise error estimates of compact difference scheme for mixed-type time-fractional Burger's equation, *Math. Comput. Simul*., **208** (2023), 702–726. https://doi.org/10.1016/j.matcom.2023.02.004
35. T. Guo, D. Xu, W. Qiu, Efficient third-order BDF finite difference scheme for the generalized viscous Burgers' equation, *Appl. Math. Lett.*, **140** (2023), 108570. https://doi.org/10.1016/j.aml.2023.108570
36. F. Safari, W. Chen, Numerical approximations for space-time fractional Burgers' equations via a new semi-analytical method, *Comput. Math. Appl*., **96** (2021), 55–66. https://doi.org/10.1016/j.camwa.2021.03.026
37. T. Wang, G. Chai, Composite spectral method for the Neumann problem of the Burgers equation on the half line, *Comput. Math. Appl.*, **134** (2023), 194–206. https://doi.org/10.1016/j.camwa.2023.01.018
38. Y. Jia, M. Xu, Y. Lin, D. Jiang, An efficient technique based on least-squares method for fractional integro-differential equations, *Alexandria Eng. J.*, **64** (2022), 97–105. https://doi.org/10.1016/j.aej.2022.08.033
39. X. Hu, S. Zhu, Isogeometric analysis for time-fractional partial differential equations, *Numer. Algor.*, **85** (2020), 909–930. https://doi.org/10.1007/s11075-019-00844-1
40. F. Soleymani, S. Zhu, Error and stability estimate of a time-fractional option pricing model under fully spatial-temporal graded meshes, *J. Comput. Appl. Math*., **425** (2023), 115075. https://doi.org/10.1016/j.cam.2023.115075
41. D. Tavares, R. Almeida, D. F. M. Torres, Caputo derivatives of fractional variable order: Numerical approximations, *Commun. Nonlinear Sci. Numer. Simul*., **35** (2016), 69–87. https://doi.org/10.1016/j.cnsns.2015.10.027
42. P. M. Prenter, *Spline and Variational Methods*, John Wiley & Sons, New York, 1975.
43. Z. Chen, *The Finite Element Method: Its Fundamentals and Applications in Engineering*, World Scientific: Hackensack, NJ, USA, 2011.
44. S. Kutluay, A. Esen, I. Dag, Numerical solutions of the Burgers' equation by the least-squares quadratic B-spline finite element method, *J. Comput. Appl. Math.*, **167** (2004), 21–33. https://doi.org/10.1016/j.cam.2003.09.043
45. A. Esen, Y. Ucar, N. Yagmurlu, O. Tasbozan, A Galerkin finite element method to solve fractional diffusion and fractional diffusion-wave equations, *Math. Model. Anal.*, **182** (2013), 260–273. https://doi.org/10.3846/13926292.2013.783884

46. M. Li, X. Ding, Q. Xu, Non-polynomial spline method for the time-fractional nonlinear Schrödinger equation, *Adv. Differ. Equations*, **2018** (2018), 1–15. https://doi.org/10.1186/s13662-018-1743-3
47. M. K. Jain, *Numerical Solution of Differential Equations*, John Wiley & Sons, New York, 1985.
48. Siraj-ul-Islam, A. J. Khattak, I. A. Tirmizi, A meshfree method for numerical solution of KdV equation, *Eng. Anal. Bound. Elem.*, **32** (2008), 849–855. https://doi.org/10.1016/j.enganabound.2008.01.003
49. A. Esen, O. Tasbozan, Numerical solution of time fractional burgers equation by cubic B-spline finite elements, *Mediterr. J. Math.*, **13** (2016), 1325–1337. https://doi.org/10.1007/s00009-015-0555-x
50. A. Esen, O. Tasbozan, Numerical solution of time fractional burgers equation, *Acta Univ. Sapientiae Math.*, **7** (2016), 167–185. https://doi.org/10.1515/ausm-2015-0011

AIMS Press